Eur. Phys. J. Plus (2017) **132**: 174
DOI 10.1140/epjp/i2017-11403-3

THE EUROPEAN PHYSICAL JOURNAL PLUS

Regular Article

Status of the crystallography beamlines at synchrotron SOLEIL*

A. Coati, L.M.G. Chavas, P. Fontaine, N. Foos, B. Guimaraes, P. Gourhant, P. Legrand, J.-P. Itie, P. Fertey, W. Shepard, T. Isabet, S. Sirigu, P.-L. Solari, D. Thiaudiere, and A. Thompson[a]

Synchrotron SOLEIL, L'Orme des Merisiers BP 48, 91192 Gif sur Yvette, France

Received: 7 February 2017
Published online: 17 April 2017 –

Abstract. Synchrotron SOLEIL (`www.synchrotron-soleil.fr`) is the French national centre for synchrotron radiation research, and has been open, for user applications, since 2008. Operating at an energy of 2.75 GeV, injected current of 500 mA, with an excellent beam stability of < 1 micron at the source position and beam "top up", and with a high proportion of straight sections for the ring circumference, SOLEIL offers a wide range of possibilities for diffraction experiments. The beamlines serving crystallographic communities are listed, along with their area of expertise and available equipment. A detailed description of the design of the PROXIMA 1 beamline for macromolecular crystallography is given, and an example of an (unsuccessful but significant) experiment is given.

1 Introduction

Synchrotron SOLEIL (`www.synchrotron-soleil.fr`) is the French national centre for synchrotron radiation research, and has been open for user applications since 2008. Operating at an energy of 2.75 GeV and a stored beam current of up to 500 mA in "top up" mode (with continuous injection of electrons keeping the stored beam current constant to within 1%), the storage ring produces an excellent beam stability of < 1 micron at the source position. The ratio of straight sections to storage ring circumference is very high, offering a wide range of possibilities for insertion devices, several of which are aimed at diffraction experiments. In 2015 the facitily was visited 4224 times, by 2378 individual users.

No less than 8 of the 29 beamlines (installed or in construction at SOLEIL) have been designed to permit diffraction measurements, either coupled to other methods (for example absorption spectroscopy or tomography) or as a dedicated method. These include measurements under extreme conditions (high pressure on the PSICHÉ beamline, radioactive samples on MARS), the use of coherent radiation (CRISTAL), the characterisation of materials (including thin films) at different energies (CRISTAL, SIXS, SIRIUS), and structure solution either for bio- or chemical crystallography (PROXIMA 1 and PROXIMA 2a).

Among the new developments underway at SOLEIL, the "femto-slicing" technique is of high interest for some of the diffraction end-stations. A laser interaction, with the electron beam, produces a slightly higher-energy electron bunch displaced with respect to the main bunch, the x-radiation resulting from this bunch will allow measurements at the few hundreds of femtoseconds timescale. Although flux is low in this mode of operation, it opens the window for pump probe diffraction measurements on very short timescales. The storage ring operation schedule varies slightly from year to year, but typically somewhere in the range of 200–220 days of beamtime are available to users, with a very high reliability (close to 99% beam availability during operations in 2015).

Full details of the diffraction beamlines at SOLEIL can be obtained by consulting the URL below[1]. As of 2016, access to beamtime occurs via twice annual calls for academic projects (February and August), reviewed by 6 peer-review committees accessible through the SOLEIL User Net set (SUNset) application[2], or using one of several trans-national access projects funded by the H2020 European program. Selection of projects is based solely on scientific excellence, as judged by these committees.

* Contribution to the Focus Point on "Status of third-generation synchrotron crystallography beamlines: An overview" edited by Gaston Garcia.

[a] e-mail: `andrew.thompson@synchrotron-soleil.fr` (corresponding author)

[1] The URL `http://www.synchrotron-soleil.fr/Recherche/LignesLumiere#Techniques` contains links to all SOLEIL beamlines, giving full information on sample environment, beam divergence, source size, energy spread, etc.

[2] `http://www.synchrotron-soleil.fr/Recherche/SUN`.

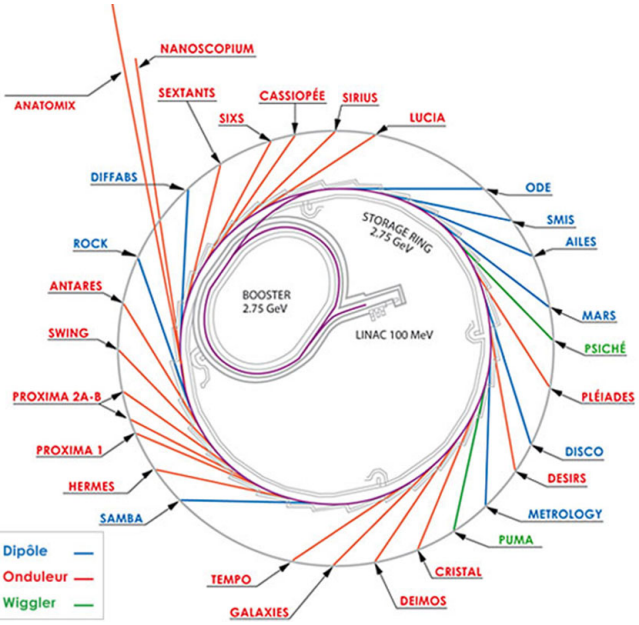

Fig. 1. Distribution of beamlines around the SOLEIL storage ring. The beamlines used for diffraction studies are mentioned in the text. © Synchrotron SOLEIL.

2 Beamlines for crystallography at SOLEIL

The specificities of the eight beamlines used for diffraction measurements at SOLEIL are reproduced, in table 1, in order to put this information in a convenient form. These include three beamlines dedicated to crystallographic measurements and structure solution (two optimized for the crystallography of biological macromolecules, and one for the measurement of coherent, time-resolved or high-resolution diffraction experiments). The remaining end-stations offer setups for diffraction measurements in several specialized applications (for example, measurements under extreme conditions, or of radioactive samples). This article includes a detailed description of one of the diffraction beamlines, the PROXIMA 1 beamline for bio-crystallography.

The distribution of the beamlines around the synchrotron radiation source is given in fig. 1. The outer circumference of the storage ring building contains laboratory facilities, which are closely linked to the beamline operation. In the context of the diffraction beamlines, for example, a high-pressure laboratory is available right next to the experimental station of the PSICHÉ beamline, which allows optimization of sample loading in different geometry diamond cells designed for the several high-pressure presses available for installation on the beamline. Additional laboratory facilities are available for the fabrication and characterization of microfluidic chips (under development as a means of delivering crystals for diffraction in the X-ray beam), for the characterization of surfaces and for the reception and preparation of biochemical or chemical samples.

3 Example of a crystallography beamline at SOLEIL — PROXIMA 1 for bio-crystallography

A U20 (20 mm period) permanent magnet undulator source delivers X-rays to the PROXIMA 1 beamline, which was one of the first beamlines opened at SOLEIL in 2008. At the time of writing, 763 released protein structures in the Protein Data Bank [1] are attributed to data collected at this beamline.

Radiation emanating from the undulator magnet passes through a cryogenically cooled channel cut Si(111) monochromator situated in a lead-lined radiation enclosure (optics hutch), and arrives in the experimental hutch, where it is focused at the sample position. The beam divergence from an undulator source is intrinsically low, and the beamline operates with both vertical and horizontal divergence significantly lower than 1 mrad (see below). Two focusing mirrors are arranged in Kirkpatrick-Baez (KB) geometry, and hence allow a separate control of the horizontal and the vertical focusing. Consequently, the mirror arrangement can be used to adapt the beam focus and divergence to the crystal unit cell under study in the vertical and horizontal diffracting directions. When coupled with a 3-circle goniometry for orienting the crystals prior to data collection, and a large surface PILATUS 6M hybrid pixel array detector, the orientation and size/divergence of the X-ray beam can be controlled precisely. In this way the beamline has been particularly successful in collecting data from very large unit cell dimension crystals (up to 750 Å in one direction).

Mechanically, the beamline is constructed in functional segments, each segment being supported by a granite plinth rigidly grouted to the experimental area floor. This construction strategy ensures both rigidity (with close to zero amplification of cultural noise between the floor and the beam conditioning elements), and ensures that all functional units stay connected on the same substructure.

Table 1. Short summary of the principal parameters of beamlines for diffraction experiments at SOLEIL. Further details (for example, beam divergence, flux, energy resolution and descriptions of sample environments) are available on individual beamline web pages, which may be consulted in English or French from the URL given in an earlier footnote.

Beamline name	Scientific domain	Radiation source	Focal spot size	Energy range	Goniometer	Detector for diffraction measurements
CRISTAL	Quasi-crystals, coherent diffraction, time-resolved diffraction, powder diffraction	20 mm period in vacuum undulator	Variable - $30 \times 450\,\mu m^2$ up to $400 \times 1000\,\mu m^2$	4–40 keV	2 circle, 4 circle κ geometry, 6 circle κ geometry heavy duty goniometer	ANDOR CCD camera. Other detectors can be installed for specific applications
DIFFABS	Diffraction and absorption measurements for materials science	Bending magnet	$\sim 10 \times 10\,\mu m^2$	3–19 keV	6 circle κ geometry heavy duty goniometer	CirPAD curved hybrid pixel array detector XPAD hybrid pixel array detector
MARS	High-resolution powder diffraction coupled with absorption spectroscopy from radioactive samples	Bending magnet	Variable - $5 \times 5\,\mu m^2$ using KB optics up to $0.3 \times 3\,mm^2$	3.5–36 keV	Heavy duty goniometer for powder diffraction, and multi-axis sample manipulator	MAR 345 image plate
PROXIMA 1	Macromolecular crystallography	20 mm period in vacuum undulator	$80 \times 25\,\mu m^2$	5.5–15.5 keV	3 circle κ geometry	PILATUS 6M
PROXIMA 2A	Macromolecular crystallography	24 mm period in vacuum undulator	$10 \times 5\,\mu m^2$	5–15 keV	Single axis ARINAX MD2	EIGER 9M
PSICHE	High-pressure diffraction, Laue diffraction	50 mm period in vacuum multipole wiggler	Variable: typically $10 \times 10\,\mu m^2$ up to $100 \times 100\,\mu m^2$. Possibility of large beam for tomography	White beam 15–100 keV, monochromatic beam 15–50 keV	CAESAR system for energy dispersive diffraction measurements	MAR345, Flat panel, Rayonnix SX165

Table 1. Continued.

Beamline name	Scientific domain	Radiation source	Focal spot size	Energy range	Goniometer	Detector for diffraction measurements
SIRIUS	Diffraction and spectroscopy from soft matter or interfaces and semiconductor nanostructures	36 mm period Apple II undulator	Variable between $3 \times 1\,\mathrm{mm}^2$ to $100 \times 100\,\mu\mathrm{m}^2$ according to application. Focussing ($< 10 \times 10\,\mu\mathrm{m}^2$) optics under construction.	1.4–13 keV	7-circle diffractometer, 2 detector arm, with Langmuir trough, controlled atmosphere chamber and under vacuum chamber/In vacuum 4-circle goniometer (under construction)	2D: PILATUS 1M 1D: Gas filled detector Fluorescence: 1 element and 4 elements Brüker, diodes and solid detectors (YAP)
SiXs	Surface X-ray scattering and diffraction, Grazing incidence diffraction	20 mm period in vacuum undulator	$40 \times 25\,\mu\mathrm{m}^2$ at Multi-environment diffractometer (MED), $30 \times 25\,\mu\mathrm{m}^2$ at UHV goniometer	5–20 keV	Multi-environment diffractometer, UHV diffractometer coupled to fabrication and characterization chambers.	X-PAD hybrid pixel array detector (soon EIGER 1M)

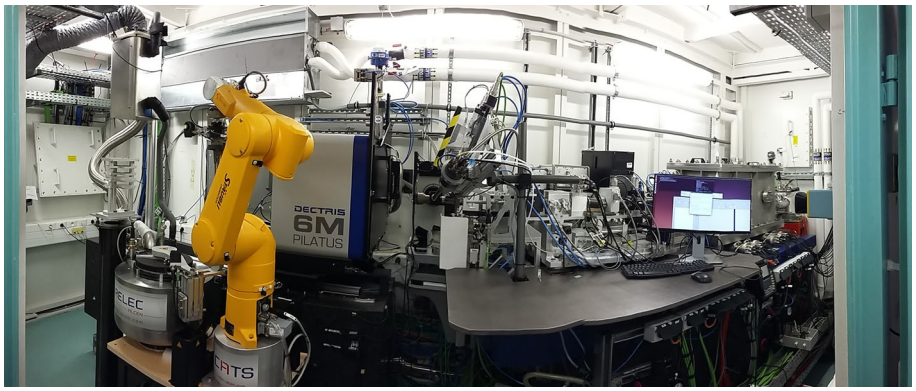

Fig. 2. Experimental end-station of the PROXIMA 1 beamline at SOLEIL. The X-ray beam arrives from the right-hand side of the image, passing through the KB mirror chamber. In the setup used, the beam is either focused at the goniometer, on the surface of the detector, or simply collimated. The goniometer and mirror assembly are installed on a metal frame supported by the same granite block (not visible on the picture), allowing a very rigid support yet with enough flexibility to track beam movements using a jacking system under the metal frame. The sample changer robot can be seen to the left of the image.

In order to both reduce the beam divergence for very large unit cell dimension crystals at the same time as reducing beam intensity to limit radiation damage to sensitive biological crystals (following a protocol inspired from [2]), the intrinsically low horizontal divergence of the beam (0.35 mrad) is further reduced by focusing the incoming X-rays at or behind the detector, the vertical beam divergence being naturally significantly smaller (0.1 mrad). The beamline layout in the experimental hutch is shown in fig. 2.

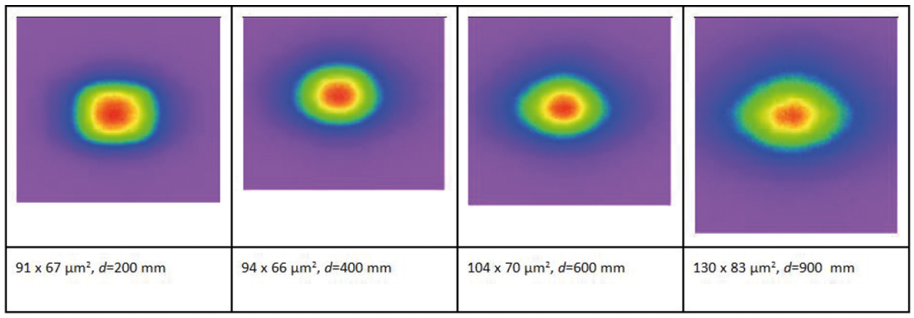

Fig. 3. Images of the focused X-ray beam (prior to beam defining apertures which limit the beam, and prior to improved optics which enable a vertical spot size of 15 μm to be achieved) at different distances from the sample position, collected on PROXIMA 1 using a Basler camera coupled to a YAG:Ce disk via an objective lens. The point-spread function of the camera is approximately 15 μm. Full width half maximum (FWHM) image sizes are given for each image. The very low beam divergence in both horizontal and vertical can be inferred from these numbers.

The beam focusing mirrors are based on the bimorph design [3], made from multi-element piezo-electric actuators, which can deform a pre-figured surface mirror shape to make elements of the X-ray wavelength coalesce to a fine focus. In the case of PROXIMA 1 the surface shape of the mirror can be varied by changing the voltage supplied to each piezo element of the bimorph mirrors, and consequently establish a look up table of voltages which can be applied to choose different focal positions and selecting different portions of the beam to give a uniform profile for a large depth of focus (see fig. 3). The most useful setting, suggested earlier by the parallel beam mode operation favored at beamlines in DESY PETRA-III [4] has been shown to be a "quasi-parallel" beam (in our case the closest we can get to true parallel beam is obtained by adjusting the divergence to be as low as 56 μrad in the horizontal direction and after the focus). The volume of crystal sample illuminated by the beam thus produced can be modified by inserting different sized horizontal apertures (availability of 90 μm, 40 μm and 25 μm, respectively) in front of the crystal, with only minor effects on the beam divergence. Consequently, the spot-to-spot resolution of the diffraction pattern becomes well defined, a major point when experimenting on large unit-cell crystals. The typical shape of the X-ray beam, remains nearly identical for a given optimized mirror curvature and sample defining slit geometry, as measured by a monitoring system made from a single YAG crystal, objective, and camera [5] at different distances after the focus. Consequently the X-ray beam on PROXIMA 1 can be adapted by a combination of focusing (defining the vertical beam size) and aperture (using the minimum horizontal aperture described above) systems to a minimum size of approximately 25 μm^2 at the sample and up to a maximum size of nearly 130 $\times$ 100 μm^2.

A flux-calibrated X-ray–sensitive photodiode was used to calculate the X-ray beam flux over a variety of energies and for the above focus conditions. A number of measurement points for different sample position apertures, various combinations of attenuating foils, and for a variety of beam currents have been established. Flux measurements were coupled with visual Basler camera images (a visible light rapid framing detector with X-rays converted to light via a single YAG:Ce crystal) giving both the beam size and shape for every intensity setting. The intensities resulting from these measurements were incorporated into a software device that interrogates the beamline settings and returns both beam size and flux at the sample position.

This precise conditioning of the X-ray beam, together with careful calibration of the dose delivered at the sample position, were key features that enabled further studies of intricate macromolecular assemblies, such as the eukaryotic ribosome in complex with different inhibitors studied at higher resolution (2.8 Å) [6] when compared to the native structure reported earlier [2].

The multi-circle goniometer presents another exceptional feature of a beamline for macromolecular crystallography. The kappa (κ) geometry for X-ray crystallography was introduced for the CAD4 system by Nonius[3]. An increasing number of beamlines are being equipped with modified versions of this type of goniometry, the so-called "mini kappa" systems [7]. Relatively few macromolecular end-stations opted for a full goniometer, mostly because of space and shadow constraints, but also as a result of the unfamiliarity of users with this geometry that can lead to physical hardware collisions between the goniometer and surrounding equipment. PROXIMA 1 has been equipped with such a large dimension goniometer (Crystal Logic, Ltd.). The instrument comprises a horizontal geometry ω-axis allowing full rotation, but which is, in practice, confined to operating between $-90°$ and $+90°$ to limit any possibility of collisions; a κ-axis inclined at an α angle of 50° and with an angular range covering $\pm 55°$; and a ϕ-axis opening to a full 360° rotation of the sample. Anti-collision monitoring is provided by a programmable logic controller, which continually surveys[4] all permitted motor positions from the goniometer depending on the detector distance from the

[3] See `http://www.nonius.nl/cad4/manuals/user/chapter02.html`.

[4] The anti-collision mechanism described in the text is an in-house development at SOLEIL. Details are available from the authors.

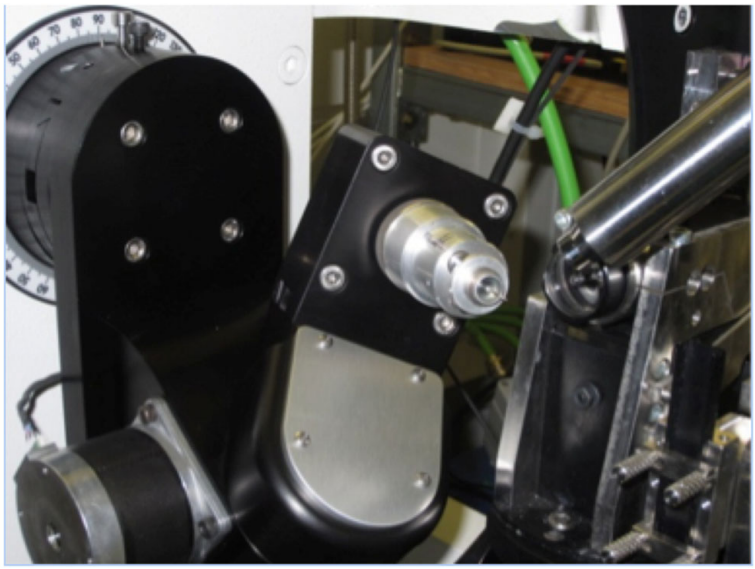

Fig. 4. The crystal logic goniometer on the PROXIMA 1 beamline. The large air bearing stage which comprises the ω rotation (black, ω angle set to -90°) supports a κ-axis (set to $+30^\circ$). The goniometer geometry, as well as the first implementation of this type of goniometer are defined as per `http://www.nonius.nl/cad4/manuals/user/chapter02.html`. The ϕ rotation turns the low profile goniometer "head"; this device is based on a tripod, allowing the sample to be "tilted" (translated) into the X-ray beam as well as a large range of movements along the ϕ-axis to adapt the height of the sample above the rotation axis.

sample position. When collision menaces, the monitoring system stops all motor movements, imposing a manual reset of the situation so that the origin of the detected collision condition be examined prior to re-enabling the movement. Meanwhile, and in order to minimize the possibilities to place the sample environment in such a risky situation, the graphical user interface understands and analyses all requested motor positions, avoiding any unsafe state of the system. The combination of these measures has led to a very reliable operation of the goniometer with collisions extremely rare (and only produced in the hands of "experts" who override the safety system!).

At PROXIMA 1, data collection is possible either using ω or ϕ scan. To facilitate the design of data collection strategies, as well as to permit user-friendly analysis of the collected images, a series of algorithms have been developed at the beamline (P. Legrand, unpublished), allowing for complicated yet well-thought strategies of data collection using the full potential of the κ goniometry. Thus, the calculation of the ϕ rotation axis vector after an offset in the κ angle (see fig. 4) is facilitated, followed by reduction of the data (based on the use of the `XDS` program [8]) collected around the ϕ-axis for non-zero κ values. This combination of movements makes the goniometer a particularly flexible instrument and allows the user to adapt data collection protocols to the required experiment.

4 Experimental case study: Phasing experiments using weak anomalous signal

The combination of the capabilities of the multi-circle goniometer, the careful control of beam intensity described above, and the unique properties of the hybrid pixel array detector in place offers the possibility of measuring very highly redundant diffraction data collected around different rotation axes, particularly effective in phasing from the very tiny anomalous signals resulting from the S atoms in methionine and cysteine residues (S-SAD phasing). The first successful S-phasing experiment on the PROXIMA 1 beamline, using data collection around multiple rotation axes to help obtaining "true redundancy" was determined from a data set collected on the ADSC Q315r CCD detector [9]. To set the current limits of the technique, the present report herein describes an unsuccessful experiment, which occurred in 2010, which underlined the potential of the method while encouraging the beamline team to further develop strategies and improved instrumentation for accurate data collection, around multiple axes, from crystals exhibiting weak anomalous signal at longer wavelenths.

MatP (Macrodomain Ter) is an 18 kDa protein expressed in Escherichia Coli and involved in chromosome condensation. MatP structure and its complex with the matS Ter signature DNA sequence were initially reported (see [10]), followed by the crystal studies of similar complexes [11] on the PROXIMA 1 beamline. Most interestingly, the 23-mer matS duplex DNA contains 46 phosphate moieties, added to 4 sulfur atoms from the four Met residues in the sequence of MatP. The presence of so many native anomalous S and P atoms from the complex when positioned at lower energies was expected to yield a large anomalous signal for low energy SAD phasing, an approach of high interest since, despite numerous efforts including Se-met incorporation, no well-diffracting heavy atom derivative was available for

Table 2. Summary of data processing statistics for the 4 data collections and the merged data that forms the final set. The 5t data set was only used as a reference for scaling purposes and consequently does not figure in the merged statistics. Data were reduced with the XDS program [8] that consequently defines the statistics reported here; R_{meas} (redundancy independent R factor, as described in [15]) is a measurement of the reliability of the data and describes the fractional difference in equivalent intensities (corrected for the number of observations) normalized to the average intensity in a resolution shell, SigAno (mean anomalous difference normalized by its estimated standard deviation), $I/\sigma(I)$ (mean of the ratio of intensity divided by standard deviation for unique reflections and after merging of symmetry related reflections). * The multiplicity, for the 3 datasets recording the S and P anomalous signal, counts F^+ and F^- as separate reflections, whereas the value for 5t does not (and consequently no SigAno value is quoted for this data set).

Data set	$\Delta\phi$ (°)	Oscillation axis/range (°)	λ (Å)	κ (°)	ϕ (°)	R_{meas} (%)	$I/\sigma(I)$	SigAno*	Multiplicity*
2t	0.5	ω/180.5	1.907	18.5		6.5 (110.6)	21.3 (1.4)	1.59 (0.96)	7.2
3t	0.5	ω/180.5	1.907	8.5		6.7 (156.1)	20.5 (1.0)	1.61 (0.67)	7.1
4t	0.5	ϕ/658	1.907	0	0	10.0 (311.1)	27.0 (0.9)	1.12 (0.65)	27.4
5t	0.5	ϕ/80	0.98	0	0	7.2 (271.9)	13.72 (0.5)	–	4.8
Merged (2t-3t-4t)						5.2	30.4 (1.23)	2.01 (0.67)	41.6 (24.3)

experimental structure determination. Historically, although the successful use of the P signal for anomalous phasing has been described [12], relatively few examples of successful application of this method exist. On the contrary, in the present study the expected 46 phosphate groups and 4 S sites were expected to provide a major challenge for locating the heavy atom sites. The strategy advocated here was to attempt improving data quality from collecting very high-redundancy data around multiple crystal orientations, which could offset these difficulties.

The data were collected on a large crystal ($\sim 150 \times 50 \times 50\,\mu\mathrm{m}^3$) with the horizontal X-ray beam reduced to approximately $40\,\mu$m as described above, and at a wavelength of 1.91 Å. With this setup, an anomalous scattering factor contribution of 0.83 e- and 0.65 e- for S and P atoms, respectively, can be calculated. Initial indexing of the crystal assigned a tetragonal system in the 422 point group, with unit cell dimensions of $a = b = 74.62$ Å, $c = 227.29$ Å, $\alpha = \beta = \gamma = 90°$. The crystal was aligned using the κ and ϕ rotations, so that the c^*-axis ran along the ω-direction allowing the collection of Bijvoet pairs continuously as the sample was rotated. A further data set at a different sample orientation was collected in order to change the beam path through the crystal to fill the gap of the data not collected because of the detector module geometry. These data collections were followed by translation of the crystal to a fresh and non-exposed area, allowing for the collection of two additional data sets at different κ offset angles (including one data set collected at 0.98 Å wavelength to provide a low absorption error reference data set for scaling purposes). Data collection quality and statistics, to a diffraction limit of 2.7 Å resolution from these 4 crystal settings together with the statistics from a merged data set are reported in table 2. When combined the overall dataset gave highly complete (99.8%) and redundant (each reflexion was measured on average 41.6 times counting Friedel mates as separate reflexions). The Matthew's coefficient, as calculated via the `CCP4` program suite [13,14], indicated the likely presence of two complexes in the asymmetric unit, indicating a total of 92 potential "phosphate super atoms" and 8 S atom positions to assign prior to structure solution.

Attempts to solve this complicated anomalous partial structure for several different combinations of asymmetric unit content, different resolution cutoffs for the data, seeding the solution by the expected distance between phosphate groups in double stranded DNA, and different scaling methods, failed to reveal any interpretable solution. On publication of an almost identical crystal structure by another group (PDB accession code 4d8j; [10]), the solution of the structure could be obtained by the molecular replacement method using the program `PHASER` [16]. The correct space group appeared to be $P4_32_12$, in which a dimer of the MatP protein bound to a single 23mer double-stranded DNA molecule could be identified, consequently accompanied by a high solvent content. Full refinement of the structure was not performed, however initial analysis suggested high B factors with a region of disorder at the N-terminal part of the protein. This unresolved structure resulted in a lack of anomalous signal as indicated by the peak heights in an anomalous Fourier synthesis for two out of the four Met S atoms. Although the localization of the heavy atom sites *ab initio* did not succeed, the solution of the structure determined based on the known positions (extracted from the partially refined molecular replacement solution and verified by anomalous Fourier synthesis) of P and S atoms was successful, indicating the intrinsic quality of the anomalous signal. Figure 5 shows an anomalous Fourier map, with contour level starting at 4.1σ, clearly identifying the double helical phosphate backbone resulting from the DNA on the top of the S atoms from the ordered Met residues.

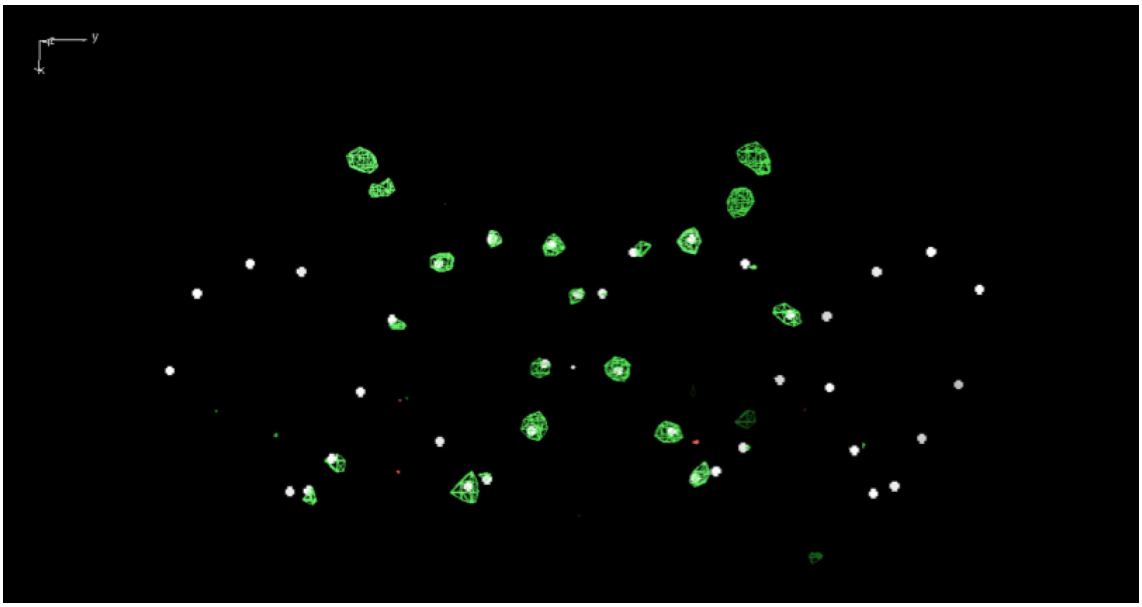

Fig. 5. Screenshot from the COOT software [17]. The white points represent the assigned positions to the phosphate groups of the double-stranded DNA in the partially refined structure, the green density representing the contoured anomalous Fourier map (contour level starting at 4.1σ). The peaks not associated with the DNA are those of the well-ordered Met residues in the MatP protein close to where it binds the DNA. The height of the Fourier peaks decreases markedly towards the two ends of the DNA molecule, *i.e.* away from the binding interface.

A generalized approach to native SAD (stimulated by the ideas reported in [18]), using the PriGo goniometer and the hybrid pixel array PILATUS detector, has been reported at the Swiss Light Source [19], describing the successful use of the method to solve a number of structures from chemically unmodified samples. Indeed, the use of photon counting detectors coupled with data collection from multiple crystals has rendered native SAD phasing reliable to the point at which it can be considered as an alternative to producing delicate Se-Met marked proteins when sufficient quantity of well enough diffracting crystals are available. It should be noted that the success rate for S-SAD phasing experiments increased significantly with the installation of the PILATUS detector at PROXIMA 1 in 2011, owing to the improved signal to noise performance which allows collecting data with reduced doses. Several structures have been solved on the PROXIMA 1 beamline employing this approach (see, for example, [20,21] and [22]), even extended it to the use of the anomalous signal from S atoms as an aid to correct ambiguous tracing of electron density maps (discussed in the case of the RNA polymerase 1 structure reported in [23,24]). Unfortunately, due to lack of reproducibility of crystals, it has not been possible to demonstrate that the unsuccessful structure solution of MatP would have succeeded with the more sensitive detection system and improved signal to noise performance on the beamline, but the excellence of the electron density map as phased using the P anomalous signal suggests that this would have been the case.

5 Conclusion

SOLEIL offers both beamline and ancillary facilities for a wide range of diffraction experiments. The performance of the PROXIMA 1 beamline for macromolecular crystallography has benefited from the reintroduction of multi-circle goniometry which, when combined with state-of-the-art pixel array detectors, has led to routine usage of the beamline for native SAD phasing experiments.

AT would like to acknowledge all the staff at SOLEIL (not only providing support on the beamlines but also providing the stored beam, software, electronics, infrastructure and administrative support for our users) and the synchrotron user community who produce so much excellent science. The FP7 project BioSTRUCT-X (contract number 2835760) is thanked for support of dissemination and training actions, and in particular for funding meetings of the kappa working group, an inter synchrotron group devoting effort to hardware and software solutions for the implementation of multi-circle goniometry at MX beamlines, and ably led by Sandor Brockhauser.

References

1. H.M. Berman, J. Westbrook, Z. Feng, G. Gilliland, T.N. Bhat, H. Weissig, I.N. Shindyalov, P.E. Bourne, Nucleic Acid Res. **28**, 235 (2000).
2. A. Ben Shem, N. Garreau de Loubresse, S. Melnikov, L. Jenner, G. Yusupova, M. Yusupov, Science **334**, 1524 (2011).
3. R. Signorato, J.-F. Carré, T. Ishikawa, Proc. SPIE **4501**, 76 (2001).
4. G. Bourenkov, *DESY Beamline P14*, private communication.
5. M. Bordessoule, J. Phys. Conf. Ser. **425**, 192018 (2013).
6. N. Garreau de Loubresse, I. Prokhorova, W. Holtkamp, M.V. Rodnina, G. Yusupova, M. Yusupov, Nature **513**, 517 (2014).
7. S. Brockhauser, R.B.G. Ravelli, A. McCarthy, Acta Cryst. D **69**, 1241 (2013).
8. W. Kabsch, Acta Cryst. D **66**, 125 (2010).
9. A. Goulet, G. Vestergaard, C. Felisberto-Rodrigues, V. Campanacci, R.A. Garrett, C. Cambillau, M. Ortiz-Lombardía, Acta Cryst. D **66**, 304 (2010).
10. P. Dupaigne, N.K. Tonthat, O. Espeli, T. Whitfill, F. Boccard, M.A. Schumacher, Mol. Cell **48**, 560 (2012).
11. D. Durand, I. Li de la Sierra-Gallay, M.A. Brooks, A. Thompson, N. Lazar, J. Lisboa, H. Van Tilbeurgh, S. Quevillon-Cheruel, Acta Crystallogr. F **68**, 638 (2012).
12. Z. Dauter, D.A. Adamiak, Acta Cryst. D **57**, 990 (2001).
13. Collaborative Computational project, Acta Cryst. D **50**, 760 (1994).
14. M.D. Winn, C.C. Ballard, K.D. Cowtan, E.J. Dodson, P. Emsley, P.R. Evans, R.M. Keegan, E.B. Krissinel, A.G.W. Leslie, A. McCoy, S.J. McNicholas, G.N. Murshudov, N.S. Pannu, E.A. Potterton, H.R. Powell, R.J. Read, A. Vagin, K.S. Wilson, Acta Cryst. D **67**, 235 (2011).
15. K. Diederichs, A. Karplus, Nat. Struct. Biol. **4**, 269 (1997).
16. A.J. McCoy, R.W. Grosse-Kunstleve, P.D. Adams, M.D. Winn, L.C. Storoni, R.J. Read, J. Appl. Cryst. **40**, 658 (2007).
17. P. Emsley, B. Lohkamp, W. Scott, K. Cowtan, Acta Crystallogr. D **66**, 486 (2010).
18. Q. Liu, T. Dahmane, Z. Zhang, Z. Assur, J. Brasch, L. Shapiro, F. Mancia, W.A. Hendrickson, Science **336**, 1033 (2012).
19. T. Weinert, V. Olieric, S. Waletrsperger, E. Panepucci, L. Chen, H. Zhang, D. Zhou, J. Rose, A. Ebihara, S. Kuramitsu, D. Li, N. Howe, G. Schnapp, A. Pautsch, K. Bargsten, A.E. Prota, P. Surana, J. Kottur, D.T. Nair, F. Basilico, V. Cecatiello, S. Pasqualato, A. Boland, O. Weichenreider, B.C. Wang, M.O. Steinmertz, M. Caffrey, M. Wang, Nat. Methods **12**, 131 (2015).
20. S. Klinke, N. Foos, J.J. Rinaldi, G. Paris, F.A. Goldbaum, P. Legrand, B.G. Guimarães, A. Thompson, Acta Cryst. D **71**, 1433 (2015).
21. A. Nawrotek, B.G. Guimarães, J. Velours, A. Subtil, M. Knossow, B. Gigant, J. Biol. Chem. **289**, 25199 (2014).
22. S. Trowitzsch, C. Viola, E. Scheer, S. Conic, V. Chavant, M. Fournier, G. Papai, I.O. Ebong, C. Schaffitzel, J. Zou, M. Haffke, J. Rappsilber, C.V. Robinson, P. Schultz, L. Tora, I. Berger, Nat. Commun. **6**, 6011 (2015).
23. C. Fernandez-Tornero, M. Moreno-Morcillo, U.J. Rashid, N.M.I. Taylor, F.M. Ruiz, T. Gruene, P. Legrand, U. Steuerwald, C.W. Müller, Nature **502**, 644 (2013).
24. M. Moreno-Morcillo, N.M.I. Taylor, T. Gruene, P. Legrand, U.J. Rashid, F.M. Ruiz, U. Steuerwald, C.W. Müller, C. Fernández-Tornero, Acta Cryst. D **70**, 2570 (2014).